

Adsorption of oxygen on Cu(100). II. Molecular adsorption and dissociation by means of O *K*-edge x-ray-absorption fine structure

T. Yokoyama,* D. Arvanitis, T. Lederer, M. Tischer, L. Tröger, and K. Baberschke
Institut für Experimentalphysik, Freie Universität Berlin, Arnimallee 14, D-14195 Berlin, Germany

G. Comelli

Sincrotrone Trieste, Padriciano 99, I-34012, Trieste, Italy

(Received 29 March 1993; revised manuscript received 23 July 1993)

The structural and dynamical properties of molecular oxygen in submonolayer coverage adsorbed on Cu(100) were investigated by means of oxygen *K*-edge photoabsorption. The adsorption geometry of the O₂ molecules, as well as the disorder and anharmonic contributions to the pair distribution function for the first-nearest-neighbor O-Cu shell were quantitatively determined for well-defined sequential molecular states of physisorption and chemisorption. The O₂ molecules are found to adsorb in a tilted configuration. Furthermore, the O-Cu interatomic pair potentials are estimated. It is found that the nearest-neighbor O-Cu bond varies only slightly as the strength of chemisorption increases, in opposition to a strong O-O bond length and other O-Cu pair-potential parameter variations.

I. INTRODUCTION

The understanding of the sequential process of physisorption, chemisorption, and dissociative atomic adsorption constitutes a fundamental step towards the understanding of the interaction between gases and solid surfaces. For several adsorbate-substrate systems such a sequence of adsorption events could be verified experimentally. In particular for oxygen molecules in submonolayer coverage on Pt(111) (Ref. 1) two well-defined sequential molecular states were found; a physisorbed state which is stable around 30 K or lower will be converted into a chemisorbed state upon heating to ~ 150 K. It was revealed by O *K*-edge near-edge x-ray-absorption fine structure (NEXAFS) studies^{2,3} on this system that in the physisorbed state the O₂ molecule is structurally unperturbed and paramagnetic. In contrast, in the chemisorbed state the O-O distance is stretched by 0.16 Å, and the O₂ magnetic moment is strongly reduced through the interaction with the substrate.^{1,3} The O₂/Ag(110) system also provides trapped physisorbed and chemisorbed molecular states, and has been studied experimentally^{2,4-7} and theoretically.^{8,9} For the chemisorbed state, the O-O distance is found to be elongated by as much as 0.26 Å (Ref. 2) and the O-O vibrational frequency is significantly lowered.^{6,7} Theoretical calculations⁹ proposed for this system that the dissociation process from the chemisorbed state takes place with little variation in the O-Ag bond length, implying that the relevant reaction coordinate for the dissociation process should lie mostly along the O-O bond direction. The adsorbate-substrate interactions are still not completely understood. Most of the structural information is given on the O-O bond distance or vibrational frequency. Direct experimental information on the adsorbate-substrate bond length and local geometry is still missing in all the cases of O₂ adsorption.

In the present study, we investigate the adsorption of

O₂ on Cu(100). It is found by the present thermal desorption spectroscopy, x-ray photoelectron spectroscopy, and NEXAFS measurements that this system gives also the well-distinguished physisorbed and chemisorbed phases as for O₂/Pt(111) and O₂/Ag(110). Furthermore, we analyzed also the surface-extended x-ray-absorption fine structure (SEXAFS) for both the physisorbed and chemisorbed molecular states. This is, to our knowledge, the first investigation which successfully provides direct structural information on the adsorbate-substrate interaction for physisorbed molecular states. In combination with the NEXAFS results on the same samples, the adsorption geometries of the O₂ molecules are quantitatively determined and compared to the one of atomic adsorption states, which allows one to associate a structural picture with the dissociation process. Furthermore, the adsorbate-substrate interatomic potentials are estimated for the molecular states and compared to one for the atomic adsorption state which has already been investigated in detail by means of SEXAFS measurements.^{10,11}

The present paper is structured as follows. In Sec. II, experimental details are given for the sample preparation and synchrotron-radiation-based measurements. Section III deals with the results of thermal desorption spectroscopy (TDS), O *K*-edge NEXAFS and O 1s x-ray photoelectron spectroscopy (XPS), and the discussion about adsorption state identification and molecular orientation. The detailed analysis of the SEXAFS, the determined structural parameters, the adsorption geometries, and the O-Cu interatomic pair potentials are discussed in Sec. IV. Concluding remarks are given in Sec. V.

II. EXPERIMENT

All the soft x-ray spectroscopic measurements were carried out using the SX-700/I and SX-700/II monochromators at the storage ring BESSY. A Cu(100) single crystal was mounted in a conventional ultrahigh-vacuum

(UHV) chamber whose base pressure was $\sim 1 \times 10^{-8}$ Pa, and was cleaned *in situ* by repeated cycles of Ar^+ bombardment and annealing at ~ 600 K. The surface cleanliness and order were monitored with Auger electron spectroscopy (AES) and low-energy electron diffraction (LEED).

The clean Cu(100) crystal was exposed to O_2 by filling the UHV chamber directly with gas. Four different adsorption states could be prepared in submonolayer coverage, depending on the O_2 dosis and the sample temperature. Those are listed below. The labels used in order to denote the adsorption states as well as the coverage estimates are based on the results of the spectroscopic studies and will be justified in Sec. III. The following adsorption states were prepared.

(i) A molecular “physisorbed” state obtained by the exposure to submonolayer amounts of O_2 at $T \leq 44$ K. No well-defined LEED patterns could be observed except for the Cu(100) (1×1) spots with a higher background. For the data presented here, this adsorption state was prepared at $T = 25$ K and the oxygen coverage was 0.7 monolayer (ML).

(ii) A molecular “chemisorbed” state obtained by the exposure to O_2 between $T \approx 44$ and 100 K. This state can also be prepared by annealing the physisorbed state above ~ 44 K. No extra LEED patterns were detected. Here, we use the annealing procedure, by heating the physisorbed state up to 60 K. The oxygen coverage was 0.4 ML.

(iii) An atomic adsorption state corresponding to an unreconstructed Cu surface. A dosis of 300-L (where $1 \text{ L} = 10^{-6}$ Torr s) O_2 was used at 300 K. We denote this state as the “precursor” state. Broad LEED spots were observed around the positions corresponding to a $c(2 \times 2)$ structure. The oxygen coverage was 0.4 ML.

(iv) An atomic adsorption state corresponding to a reconstructed Cu surface. A dosis of 1200-L O_2 was used at 500 K. This state can be obtained also by annealing the precursor state or by using a much higher O_2 dosis at 300 K. A sharp $(\sqrt{2} \times \sqrt{2})R45^\circ$ LEED pattern was observed. The oxygen coverage was 0.5 ML.

Oxygen *K*-edge NEXAFS and SEXAFS spectra for both physisorbed and chemisorbed molecular states were taken at normal (90°) and grazing (20°) x-ray incidence angles at a temperature of 25 K by means of partial electron yield detection. We use also the SEXAFS data of the atomic precursor state taken at 50 K as a reference in the analysis. The complete SEXAFS analysis for these states is given elsewhere.¹¹ As a reference for the NEXAFS data, the spectra of an oxygen multilayer (> 25 ML) were also recorded. Oxygen *1s* XPS measurements for the two molecular states and the precursor state were performed by use of synchrotron radiation. The photon energy employed was 610 eV, and the binding energy was measured with respect to the Cu Fermi level.

III. ADSORPTION STATE IDENTIFICATION AND MOLECULAR ORIENTATION

Figure 1 shows the TDS results of O_2 molecules from $\text{O}_2/\text{Cu}(100)$ taken using a quadrupole mass spectrometer

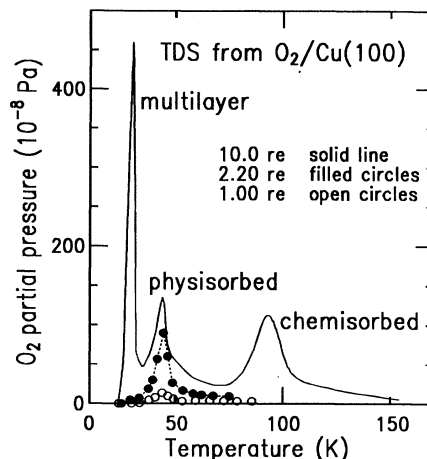


FIG. 1. Thermal desorption spectroscopy (TDS) measurements are shown for $\text{O}_2/\text{Cu}(100)$. The gas was dosed at $T = 25$ K. The crystal was subsequently heated up with a rate of ~ 2 K/s in front of a quadrupole mass spectrometer. The mass 32 was detected. Up to approximately 2 relative exposure (re) units, no multilayer formation was observed.

($m/e = 32$) in the temperature range 25–155 K with the heating rate of 2 K/s. The initial amounts of dosed O_2 in the TDS experiments were 10, 2.2, and 1.0 relative exposure (re). In the spectrum corresponding to the highest coverage (10 re) three distinct peaks can be seen at 30, 44, and 94 K, while in the spectra of the lower coverages (2.2 and 1.0 re) only one desorption peak is found around 45 K. In the subsequent studies of the physisorbed state, care was taken to use a sufficiently low coverage (~ 2 re) in order to avoid multilayer formation. The spectral features of the highest coverage closely resemble those from $\text{O}_2/\text{Pt}(111)$ reported by Luntz, Grimblot, and Fowler.¹ We can assign these three peaks to the desorption of an oxygen multilayer (30 K), physisorbed oxygen (44 K), and chemisorbed oxygen (94 K), as in the case of $\text{O}_2/\text{Pt}(111)$.

The desorption temperatures of multilayer and physisorbed oxygen are essentially the same as those from $\text{O}_2/\text{Pt}(111)$ (30 and 45 K, respectively), while the desorption temperature of chemisorbed oxygen on Cu(100) is much lower than the one of $\text{O}_2/\text{Pt}(111)$ (130 K) (Ref. 1) and also of $\text{O}_2/\text{Ag}(110)$ (190 K).⁵ From the desorption peaks for the chemisorbed states assuming first-order kinetics, one would conclude that the O_2 molecules on Cu(100) are not as strongly chemisorbed as on Pt(111) or Ag(110). The previous assumption, however, leads to a contradiction when compared to the other spectroscopic results, which indicate a strong chemisorption as in the case of Ag(110). Since the dissociation of O_2 molecules already occurs in this temperature range, the TDS peak around 100 K is the result of higher-order kinetics (recombination of the O atoms).

Figure 2 shows the O *K*-edge NEXAFS spectra for a multilayer, physisorbed and chemisorbed submonolayers of O_2 on Cu(100). Using the edge-jump ratio J_R , defined as the continuum increase of the oxygen absorption with

respect to the background, the absolute coverage can be estimated by comparing the J_R value obtained with respect to the one of the $(\sqrt{2} \times 2\sqrt{2})R45^\circ$ atomic adsorption state (data not shown here).¹¹ For the multilayer O₂ data of Fig. 2 the thickness can be estimated to be >25 ML and therefore we can neglect the contribution of the first-layer O₂ molecules directly interacting with the Cu surface. The values of 0.7 and 0.4 ML are obtained for the physisorbed and chemisorbed submonolayer data. Using the angular dependence of the NEXAFS data, the formation of a multilayer at 25 K could be monitored during the measurements. This is observed for the data of Fig. 2, where the intensity of the molecular resonances shows the opposite variation as a function of the x-ray incidence angle (dashed and full lines) for the multilayer versus the submonolayer data.

For the data of Fig. 2, we obtain from the polarization dependence of the π^* resonance the orientation angle of the O₂ molecules for the multilayer O₂.¹² The obtained bond angle for the O-O axis with respect to the surface is $64^\circ \pm 10^\circ$ assuming the linear polarization factor to be 0.90 and a single-bond-angle axis with respect to the surface. This finding implies that the O₂ molecules are mostly standing up on the surface in this case. We observe two

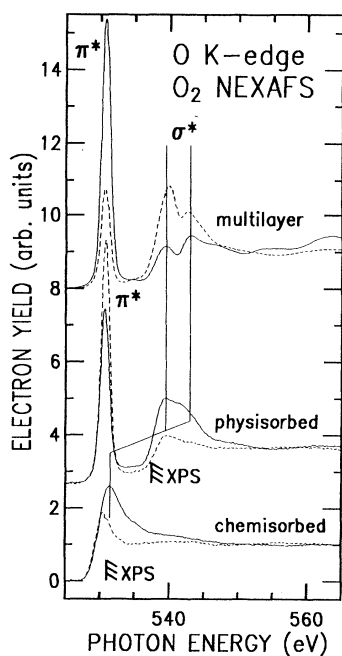


FIG. 2. The NEXAFS spectra for an O₂ multilayer, as well as a physisorbed and a chemisorbed O₂ submonolayer on Cu(100) as shown. The spectra are shown scaled to the same edge-jump ratio for the sake of comparison. The spectra of the physisorbed and multilayer species are shown after 2.7 and 8 arbitrary units have been added to the ordinate values, respectively. The data were taken at normal (full line) and 20° grazing (dashed line) x-ray incidence. The analysis of the angular dependence of the σ^* resonances of the multilayer and physisorbed states is complicated due to the superposition of Rydberg states. The XPS binding energies relative to the Fermi level are also shown for the submonolayer data.

σ^* resonances for multilayer O₂ as in the case of gaseous O₂.¹³ The splitting between the two resonances is caused by the exchange interaction of the triplet-coupled four unpaired electrons $(1s)^1(\pi_x^*)^1(\pi_y^*)^1(\sigma^*)^1$.^{3,14} The polarization dependence of these two σ^* resonances, however, does not seem to follow the one of the π^* resonance in a simple plane-orbital picture¹² as both of them should almost vanish at 90° x-ray incidence even with the imperfect degree of 0.90 for the linear polarization. Such an anomalous behavior can be understood due to the superposition of these σ^* resonances to Rydberg series as known from the gas phase.¹⁴ This superposition can be seen not only in the anomalous angular dependence but also in their relative energy, which apparently varies as a function of the x-ray incidence angle (Fig. 2). It appears therefore not straightforward to try to obtain accurate structural information from these resonances for the multilayer data in the absence of high-resolution data that would allow us to deconvolute the underlying Rydberg contributions. For the same reason, the orientation of the O₂ molecules in the submonolayer physisorbed data was derived from the π^* resonance only.

In the spectra for physisorbed O₂ of Fig. 2(b), the σ^* resonances appear at nearly the same energy as in the multilayer or gaseous O₂, indicating that the molecules in the physisorbed state are gas-phase-like and that the O-O intramolecular distance is 1.21(3) Å according to the correlation between the σ^* resonance energy and the O-O bond length.^{2,3,15} The shape, however, of the σ^* resonances appears to be different from that for the multilayer case, possibly due to the different Rydberg contributions. We therefore do not attempt to derive the O-O axis orientation from the angular dependence of these structures. The O-O tilt angle estimated from the polarization dependence of the π^* resonance is found to be $23^\circ \pm 10^\circ$. This tilt angle is consistent with those of submonolayer physisorbed O₂ on other substrates such as graphite and Ag(110) ($\approx 30^\circ$).^{4,16} The physisorbed O₂ molecules are lying mostly flat on the surface in contrast to the multilayer ones.

The lowest panel of Fig. 2 corresponds to the chemisorbed O₂ state. The spectral features are drastically changed compared to those of the physisorbed state. The σ^* resonance energy is now only 531.5 eV, considerably lower than previously, leading to the elongated O-O distance of 1.52(3) Å (stretch of 0.31 Å), a value which is a little larger than for chemisorbed O₂ on Ag(110) (stretch of 0.26 Å).² This big energy shift is accompanied by a severe reduction of the intensity of the π^* resonance (Fig. 2), revealing that the π^* states are now occupied due to bonding to the substrate. The occupation of these states with an O-O antibonding character is compatible with the energy shift of the σ^* resonance, revealing a weakening of the intramolecular bond. As a conclusion, with the π^* orbitals now almost occupied, chemisorbed O₂ on Cu(100) should be considerably negatively charged as in the case of O₂/Ag(110), whose O-O bond seems to be almost cleaved. The stretch of 0.2 or 0.31 Å is much larger than that in chemisorbed O₂/Pt(111) (0.16 Å),² indicating a stronger oxygen-substrate interaction on Cu(100) or Ag(110) than on Pt(111). The σ^* resonance is apparently

much stronger at 90° incidence, so that the O₂ molecule should lie mostly flat on the surface as in the case of physisorbed O₂. A quantitative analysis of the angular dependence of this resonance, however, is not attempted due to the complexity of the data at grazing incidence. These cannot be interpreted as due to the superposition of the π^* and σ^* states only as noticed earlier.^{3,4}

We have also measured the O 1s XPS binding energy for the molecular states. They are found to be 537.5(2) and 531.0(2) eV for the physisorbed and chemisorbed states, respectively. The XPS binding energy for the physisorbed state on Cu(100) lies between the value for the physisorbed state on Pt(111) (536 eV) (Ref. 3) and the value of the gas-phase ionization potential. It is observed that for Pt(111) as well as for Cu(100) the XPS binding energy lies well above the π^* resonance energy for the physisorbed species. This value is in agreement to the previous NEXAFS analysis of the “gas-phase-like” O₂ molecules on Cu(100) for the physisorbed state. In the case of the chemisorbed state, where the σ^* resonance position indicates strong chemisorption, the value of the XPS binding energy is close to the one found in the case of strong chemisorption on Ag(110) (529.3 eV).² Therefore for this state the XPS binding energy is consistent with the occurrence of strong chemisorption, comparable to the situation for Ag(110). It is also observed that the considerable shift in XPS binding energy of ~ 6.5 eV is stronger than the one observed for Pt(111) (4.7 eV),³ in agreement to the σ^* resonance results indicating a stronger chemisorption than for Pt(111). A supplementary absolute error of 0.6 eV (rigid shift of all values) due to the uncertainty of the incident photon energy should also be considered when compared to the photoabsorption data.

IV. SEXAFS ANALYSIS

A. SEXAFS oscillations and Fourier transforms

The normalized SEXAFS oscillations for the two molecular [curves (a) physisorbed and (b) chemisorbed] and the atomic precursor [curve (c)] states are shown in Fig. 3 at normal x-ray incidence after the free-atom background has been removed. Care was taken in order to use similar spline functions to simulate the atomic absorption coefficient for all the different data sets in order to minimize the relative errors. The corresponding Fourier transforms are shown in Fig. 4. The most intensive feature around 1.7 Å can be attributed to the nearest-neighbor (NN) O-Cu contribution. As will be discussed in detail below, the features marked by arrows for the molecular states [(a),(b)] can be attributed to the next-nearest-neighbor (NNN) O-Cu shell, the other features at higher distances can also be tentatively assigned in the framework of single-scattering theory as due to higher O-Cu shells. Their analysis goes, however, beyond the scope of the present paper as they involve structural and dynamical parameters beyond the dominant first-shell O₂/Cu₄ cluster contributions (Sec. IV C). Finally the Fourier peak around 1 Å that is observed for all adsorption states is caused by an incomplete background subtraction for the very low frequencies with also

some oxygen contribution for the molecular states, corresponding to the weak backscattering of the intramolecular O-O distance. However, due to the well-known problem in EXAFS of background-related spurious Fourier peaks at very low distances as illustrated by the atomic state data [curve (c), Fig. 4] it is hazardous to try to obtain physical information from this feature of the molecular states. It is also of importance to try to quantify eventual spurious effects on the main O-Cu frequency caused by an incomplete filtering of this low- R feature. A Hanning-type window function was used between 1.15 and 2.15 Å [Fig. 4(c)] in order to isolate the main O-Cu contribution for the atomic state. The same window function was used also for the molecular states, shifted by 0.2 Å to higher distances. Small variations in the window function (~ 0.2 Å in the window minimum and maximum values, different window strength) did not affect

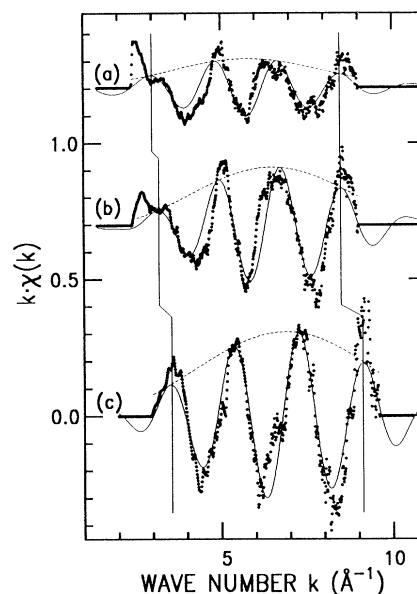


FIG. 3. The normalized SEXAFS oscillations are shown (dots) for the physisorbed (a) and chemisorbed (b) molecular states as well as for the atomic precursor state (c). These data were taken at normal x-ray incidence. The NN backfiltered oscillations after a Fourier transformation and backtransformation are shown as full thin lines. For the transformation to R space a Hanning-type window function was used between 2.4 and 9.0 Å⁻¹ for the physisorbed and chemisorbed state data and 3.0 and 9.6 Å⁻¹ for the precursor state. An alternative analysis starting from 3.5 Å⁻¹ for the physisorbed and 3.7 Å⁻¹ for the chemisorbed states yields essentially the same results. The amplitude of the backfiltered oscillations are also shown (dashed lines). A systematic phase lag between curves (a), (b), and (c) is observed at low k 's indicating a shorter NN O-Cu bond from (a) to (c) (vertical line at ~ 3.5 Å⁻¹). It is, however, observed that this lag does not increase linearly (vertical lines at ~ 9 Å⁻¹), indicating the importance of anharmonic contributions, which increase from (c) to (a). Also the amplitude maximum of the oscillations (dashed line) shifts to lower k values, indicating increasing disorder contributions for the molecular states as the binding strength to the Cu surface decreases.

the data analysis significantly, as long as these changes were performed consistently for the data of all adsorption states. The previous consistency checks give good confidence that even in the case of physisorbed molecules it is possible to extract useful information from surface EXAFS. As it is seen, however, in the data of Figs. 3 and 4 the amplitude of the SEXAFS oscillations drastically decreases as the O-Cu NN bond strength weakens, complicating the data analysis. Only through the systematic study of several adsorption states of the same system can the errors be minimized. The previous discussion illustrates also for the first time some intrinsic difficulties related to the study of weakly adsorbed molecules, related to the existence of strong disorder and intramolecular SEXAFS contributions, as to our knowledge the SEXAFS of physisorbed species has not been measured before.

Having assigned the various real-space features, we turn to a more detailed study of the NN O-Cu contributions. These are also shown after a backtransformation to k space as full lines in Fig. 3. It is clear that no good agreement between the data points (dots) and the NN O-Cu backfiltered oscillations (full lines) can be expected due to the existence of higher-shell contributions, as can

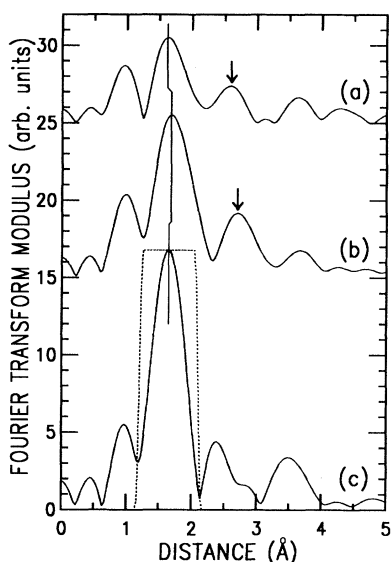


FIG. 4. The Fourier transform modulus of the SEXAFS oscillations of Fig. 3 are shown in real space. The main feature around 1.7 Å corresponds to the O-Cu NN contribution. The peak around 1 Å cannot be assigned to an O-O contribution only due to an incomplete background subtraction for the very low frequencies. The feature marked by an arrow for the molecular states [curves (a) and (b)] corresponds to the next NN O-Cu contribution in an O_2/Cu_4 cluster. As now the whole k range is sampled, the maximum position of the peaks cannot be taken as indicative of the true distance after phase-shift correction. This is mostly seen between curves (a) and (b) where an apparent contraction is observed, even if the low k region of the data (Fig. 3) clearly indicates a longer distance for (a). This effect is due to the strong anharmonic contributions that dominate at high k values.

be seen in Fig. 4. These can also be observed in Fig. 3 as the deviations between the full lines and the experiment occur in a systematic fashion corresponding to these higher frequencies. In the present study we do not only perform the conventional structural SEXAFS analysis by determining the distances R_i and effective coordination numbers $N_i^*(\Theta)$ as a function of the angle of x-ray incidence Θ , but also determine with a high degree of accuracy (1) the relative NN O-Cu bond-length changes between the different adsorption states; (2) the relative changes of C_2 and C_3 , the second and third pair distribution function (PDF) moments. The relative analysis is based only on a comparison between the different SEXAFS oscillations and is therefore assumption free as far as any structural or electronic parameters (backscattering amplitude and phase, photoelectron mean free path) are concerned.

To compare the SEXAFS oscillations of the different adsorption states at grazing or normal x-ray incidence, the k -dependent single-shell SEXAFS signal is written as

$$k\chi_{i\alpha}(k) = A_{i\alpha}(k, T)\sin\phi_i(k, T). \quad (1)$$

The first-NN shell oscillations of the different adsorption states labeled by the index i (here $i=1, 2, 3$ for three different states) are compared. The index α is necessary to designate the x-ray incidence angle only for the amplitudes $A_{i\alpha}$, as the same O-Cu bond is probed for the different x-ray incidence angles. The well-established ratio method is then used, to compare the amplitudes of the single-shell SEXAFS signals. The corresponding logarithmic ratio is given by¹⁷

$$\ln \left[\frac{A_{i\alpha}(T)}{A_{j\beta}(T)} \right] = \ln \left[\frac{N_{i\alpha}^* R_j^2}{N_{j\beta}^* R_i^2} \right] - 2 \left[\frac{R_i}{\lambda_i} - \frac{R_j}{\lambda_j} \right] - 2k^2 \Delta C_{2ij}(T), \quad (2)$$

where

$$\Delta C_{2ij}(T) = C_{2i}(T) - C_{2j}(T), \quad (3)$$

with $C_{2i}(T)$ being the second moment of the NN bond PDF of state i , related to its broadness. Equation (2) can be used not only for a ΔC_2 determination but for the ($N_{i\alpha}^*/N_{j\beta}^*$) ratio, the mean free path λ_i term inducing only a small higher-order correction. According to Eq. (2), using a logarithmic amplitude ratio plot versus k^2 , the N^* ratio and ΔC_2 of a pair of backfiltered single-shell oscillations are determined from the intercept and slope of the corresponding lines.

In a similar way the phase differences between pairs of single-shell SEXAFS signals can be analyzed:¹⁷⁻²²

$$\phi_i(T) - \phi_j(T) = k\Omega_{ij} = \frac{4}{3}k^3 \Delta C_{3ij}(T), \quad (4)$$

with

$$\Omega_{ij} = 2(R_i - R_j) - \frac{4C_{2i}}{R_i} \left[1 + \frac{R_i}{\lambda} \right] + \frac{4C_{2j}}{R_j} \left[1 + \frac{R_j}{\lambda} \right], \quad (5)$$

where

$$\Delta C_{3ij}(T) = C_{3i}(T) - C_{3j}(T) \quad (6)$$

is the difference between the third PDF moments of the NN bond, related to the asymmetry of the corresponding PDF's. The biggest contribution in the linear part of the difference is given by $R_i - R_j$, the second and third term in Eq. (5) being higher-order corrections. Using Eq. (4), if $(\phi_i - \phi_j)/k$ is plotted versus k^2 , $R_i - R_j$ and ΔC_{3ij} can be determined for a pair of backfiltered single-shell oscillations from the intercept and slope of the corresponding lines. For the present set of data anharmonic effects (i.e., $C_3 \neq 0$) have to be taken into account, even at the temperature of 25 K, due to the weakness of the O-Cu bonds for the molecular states. Their omission leads to serious mistakes for the distance determination.

The importance of these cubic contributions can even be seen by eye inspection in the NN backfiltered data of Fig. 3 (full line). A comparison of the phase of the NN contributions for curves (a), (b), and (c), corresponding to the physisorbed, chemisorbed, and atomic states, respectively, at $k \sim 3.5 \text{ \AA}^{-1}$, where the linear k contribution dominates, indicates a decreasing distance as one moves from (a) to (c) [vertical lines, Eqs. (4) and (5)]. A similar comparison at $k \sim 9 \text{ \AA}^{-1}$ indicates that curves (a) and (b) are now in phase, and that the phase lag between (a), (b), and (c) increases slower than the linear term alone would indicate [Eq. (4)]. The previous effects can be interpreted with a nonzero C_3 term that decreases from (a) to (c) as the O-Cu bond strength increases and the distance R decreases as well. The relative phase comparison indicates the importance of the k^3 term in the SEXAFS phase for a precise NN distance determination. This effect can also be followed in real space (Fig. 4) where an increase is observed in the value of the maximum of the Fourier peak going from curve (c) to (b), but a decrease going from curve (b) to (a). The high- k values due to the strength of the cubic term in the phase dominate for the physisorbed state [Fig. 4(a)], where the maximum of the Fourier transform modulus lies at lower distances than in the other states [(b), (c)] even if the linear terms at low- k values (Fig. 3) indicate a longer O-Cu distance.

The data of Figs. 3 and 4 indicate also a continuous decrease in the amplitude of the NN SEXAFS oscillations as the strength of chemisorption weakens [curve (c) to (a)]. This is caused from both the low- and high- k regions of the data (Fig. 3), indicating a continuous decrease in N^* and an increase in the C_2 values, respectively, from curve (c) to (a). The increase in C_2 is mostly seen in the shift of the maximum of the amplitude of the SEXAFS (dashed lines in Fig. 3). For the atomic state, the maximum is around 7.5 \AA^{-1} as expected from theory after the backscattering amplitude of Cu.¹⁷ A continuous decrease to low- k values is observed for curves (b) and (a) with respect to (c) revealing the importance of the increasing C_2 contributions.

B. Determination of structural parameters

Due to the large anharmonic contributions as discussed in the previous section, the commonly used harmonic SEXAFS analysis for the NN O-Cu distance deter-

mination is misleading. The amplitude and phase of the backfiltered oscillations have to be compared to the ones of a well-defined standard involving the same absorber-backscatterer pair. The analysis has to be performed by plotting the logarithmic amplitude ratios and k -divided phase differences versus k^2 . From the intercepts and slopes of these linear plots according to Eqs. (2) and (4) the distance differences, N^* ratios, ΔC_2 and ΔC_3 values are determined between pairs of backfiltered single-shell contributions. This analysis was performed for the data of the two molecular states and the precursor atomic state, for all possible pair combinations. In Fig. 5 the analysis of the O-Cu NN SEXAFS oscillations (Fig. 3, full lines) according to Eqs. (1)–(6) is exemplarily shown for two pairs of backfiltered single-shell contributions. An inspection of the data points indicates that overall the expected functional dependence in k space is observed, except for clear deviations at low- k values. The deviations of the data points from the linear laws allow one to quantify the errors in the determination of the slopes (ΔC_{2ij} , ΔC_{3ij}) and intercepts (N^* ratios, $R_i - R_j$) according to Eqs. (2) and (4). In Table I, this analysis is shown for the amplitude ratios and phase differences of

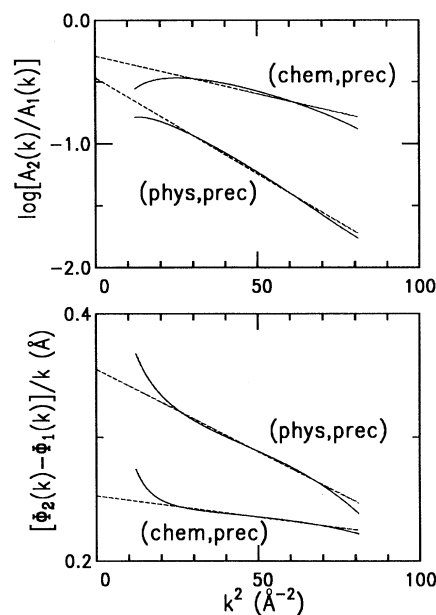


FIG. 5. The analysis of the O-Cu NN backfiltered oscillations shown in Fig. 3 is given. In the upper part the natural logarithm of the amplitude ratio is shown between the SEXAFS amplitude of the physisorbed or chemisorbed states (A_2) and the atomic precursor state (A_1), as a function of k^2 . Similarly the k -divided phase differences are shown in the lower part. The dashed lines through the data points correspond to least-squares fits. It is observed that as the O-Cu bond elongates (lower part, larger intercept) the anharmonic contributions become stronger (lower part, larger slope) and the oscillations are more attenuated (upper part, larger slope). It is observed that for both cases the logarithmic amplitude ratio (upper part) yields a similar intercept, indicating that for both molecular states the local geometry does not vary significantly.

TABLE I. Results of the single-shell SEXAFS analysis for the first NN O-Cu shell. Relative values are given with respect to the atomic precursor state based on a "generalized ratio method" (see text). The SEXAFS data of physisorbed and chemisorbed O₂ taken at an x-ray incidence angle Θ of 90° and 20° and a temperature of 25 K are compared to the data of the atomic precursor state. The N^* ratio with respect to the precursor state, the NN distance difference (ΔR), and differences in the second and third PDF moments (ΔC_2 and ΔC_3) are given. The observation of an angular dependence of ΔC_2 and ΔC_3 as a function of Θ for the chemisorbed data indicate the existence of two close-lying shells for this state.

Adsorption state	T (K)	Θ (deg)	N^* ratio	ΔR (Å)	ΔC_2 (10^{-3}Å^2)	ΔC_3 (10^{-4}Å^3)
Precursor	50	90	1.0	0.00	0.0	0.0
Chemisorbed	25	90	0.8(2)	0.14(1)	2.6(5)	2.7(5)
		20	0.9(2)	0.15(1)	5.0(5)	5.8(5)
Physisorbed	25	90	0.8(2)	0.20(2)	7.9(5)	9.9(5)
		20	0.7(2)	0.23(2)	8.2(5)	9.8(5)

the molecular states taken with respect to the atomic one. It should be noticed that this kind of analysis based on a relative comparison is assumption free, as most of the unknown SEXAFS parameters cancel out by using this "generalized ratio method." For example, the previous relative distance determination is free of any assumption on the O-Cu backscattering phase or the exact shape of the Cu backscattering amplitude. The high degree of accuracy that can be obtained for a relative determination of SEXAFS parameters (Fig. 5, Table I) is reached once a consistent analysis is performed throughout the different data sets using the same type of spline functions as well as consistent window functions in k and R spaces. Possible spurious effects induced by an eventual incomplete background subtraction or from the filtering process cancel out as only a relative analysis is performed. As a result it is observed (Fig. 5) that even in the case of the weak oscillations of the physisorbed state the data follow the expected linear laws. Deviations from the linear dependence specially at low- k values indicate the limitations of the present analysis and allow for an error determination.

Starting from the ΔR values, obtained from the intercept of the $\Delta\phi/k$ versus k^2 plots, it is observed that the distance increases continuously as the strength of chemisorption decreases. What becomes apparent, however, from the ΔC_2 and ΔC_3 values for the chemisorbed state is an angular dependence for 20° and 90°, inconsistent with the assumption of a single-shell analysis. According to Eqs. (2)–(6), in case that the same bond is probed as the angle of x-ray incidence varies, horizontal lines versus k^2 in the phase and amplitude analysis are expected. The data of Table I indicate that more than one shell is probed in this case, even if the difference in distance is very small, as indicated by the ΔR values, of the order of a few hundredths of an angstrom. Care was taken to verify this finding by analyzing all possible pair combinations of backfiltered NN contributions. It is understandable that in view of such small distance differences, no anomaly is observed in the ΔR and N^* values mostly sensitive to the linear part of the SEXAFS amplitude and phase. In contrast, ΔC_2 and ΔC_3 are sensitive to k^2 and k^3 variations, respectively, which increase the weight of

the high- k region of the data. Therefore these parameters are sensitive even to a small out-of-phase behavior between two very-close-lying shells. The enhanced accuracy of the higher PDF moments to obtain structural information is also in agreement with previous observations.^{19,21,22} Once the relative values of the different parameters of the molecular states are known, their absolute values can be determined as well, as these are known for the atomic precursor state.¹¹ For the O-Cu absolute distance determination, a value of $R = 1.86(3)$ Å is obtained for the atomic state, using an O-Cu phase shift based on a Cu₂O standard. This result is found also in good agreement with the distance obtained using a phase shift based on the *ab initio* FEFF code ($\Delta r = 0.10$ Å).²³ For this state it is also known that $N^*(90^\circ) = 3.2(2)$ as well as that $C_2 = 6.2(5) \times 10^{-3} \text{Å}^2$ and $C_3 = 4.4(5) \times 10^{-4} \text{Å}^3$.¹¹ Based on these values, also the absolute determination of the different structural parameters can be performed. It is of importance to stress the advantages of a relative analysis as the one of Table I, where the high degree of relative accuracy of the EXAFS technique ($\Delta r = 0.01$ Å) is fully exploited.

In order to further proceed with the data analysis a two-shell model has to be applied in the case of the chemisorbed state. The backfiltered oscillations of the dominant O-Cu contributions for the data of the chemisorbed state are analyzed for 90° and 20° by allowing a two-shell fit with the variable parameters N^* , R , C_2 , and C_3 for each shell, using the precursor state again as a standard. Two distances are determined yielding a $\Delta r = 0.04(2)$ Å between the two close-lying shells. The absolute values for the structural parameters obtained from this analysis are shown in Table II, together with the ones for the physisorbed state. For the physisorbed state the data of Table I do not give any hint for the existence of two separate shells in this case.

C. Adsorption geometry of the molecular states

Using the N^* values given in Tables I and II, the adsorption site of the O atoms can be determined. Due to the fact that a relative analysis is always more accurate, we examine first the polarization dependence of N^* , in

TABLE II. Summary of the structural parameters for the first NN O-Cu shell given by SEXAFS. Absolute values are given by using the data of the precursor state as a standard (Ref. 11). For the chemisorbed state the results obtained by the two-shell analysis are shown. The bigger absolute errors given here include also the supplementary error due to the absolute analysis of the precursor state data. As shown in Table I the differences between the different parameters are meaningful due to the smaller relative errors.

Adsorption state		$N^*(90^\circ)$	$N^*(20^\circ)$	R (\AA)	C_2 (10^{-3}\AA^2)	C_3 (10^{-4}\AA^3)
Precursor		3.2(3)		1.86(3)	6.2(5)	4.4(5)
Chemisorbed	Bond 1	2.5(3)	1.4(2)	1.99(3)	7.3(5)	4.6(5)
	Bond 2	0.6(2)	1.7(2)	2.04(4)	13(1)	11(1)
Physisorbed		2.4(3)	2.2(3)	2.07(4)	14(1)	14(1)

order to determine the adsorption geometry by comparing the experimentally obtained values with those calculated for different possible adsorption sites.¹⁷ Table III gives the experimentally obtained N^* ratio, $N_r = N^*(20^\circ)/N^*(90^\circ)$, for the first-NN shell, and the N^* ratio and distance for the second-NN shell appearing at $\sim 2.7 \text{\AA}$ in the Fourier transform. For the second peak of the Fourier transform [Figs. 3(a) and 3(b)] marked by an arrow, a distance around 3.2\AA was obtained (Table III) for the molecular states.

First of all we will discuss flat-lying molecule models. The O-O distance for both molecular states is taken to be the one obtained from NEXAFS (Sec. III). Here we assume that the O-O axis is parallel to the [010] (or [001]) axis, and the midpoint of the O_2 molecule is located at the hollow, bridge, or atop sites. The small midpoint displacements required from the completely symmetric configuration in order to obtain two distinct shells for the chemisorbed state do not affect the results for the N^* ratios discussed here. For small displacements yielding a $\Delta r = 0.04 \text{\AA}$ between the two close shells, no interference is observed up to $k \sim 10 \text{\AA}^{-1}$ and the N^* values of the two shells are additive. Anomalies are observed only for the higher cumulants C_2 and C_3 as discussed above. We have therefore used only symmetric geometries for the flat-lying models in order to evaluate N^* . No flat-lying models given in Table III are consistent with the experi-

mental data for the first-NN shell. If the O-O axis is still kept parallel to the surface and the O-O midpoint positioned above nonsymmetric sites is compatible with the data of Tables I and II, even bigger discrepancies are observed. Furthermore, the distance of the second-NN shells shows a clear discrepancy between the observed and calculated values. For the flat-lying models, the second-NN distance should be shorter by $\sim 0.4 \text{\AA}$. In conclusion we can exclude all flat-lying models for the O_2 molecules both for the physisorbed and chemisorbed states. This finding is found also in agreement with the analysis of the angular dependence of the π^* resonance intensity that indicates also a nonzero tilt angle for the O-O axis.

In order to explain the experimental results, a tilt model should be considered, as shown in Fig. 6. In this model we assume that one oxygen atom locates exactly at the fourfold hollow site. Then by using the data of Table II in combination with the O-O distance as obtained from NEXAFS, it can be shown that the other O atom is located close to the bridge site. For the chemisorbed state the shorter bond (bond 1) is taken to be the fourfold hollow site bond. Using the other distance (bond 2) it is calculated that the second O atom is located almost above the bridge site, the O-O axis making an angle of 30° to the surface. For the physisorbed state the same O-Cu distance is used for both O atoms, assuming one of them is

TABLE III. Comparison of the experimental SEXAFS results for the first and second NN O-Cu shells with several possible adsorption models. c is the N^* ratio, $c = N^*(20^\circ)/N^*(90^\circ)$. The quantity N_r for the first NN shell in the chemisorbed state is given in two different manners. As mentioned in the text, for the N^* values of the chemisorbed state a single-shell analysis can be assumed, and therefore the values given in Table I can be used. For the tilt model, the ratio of the sum of the N^* values of the two shells is compared to the experimental result. It is observed that the tilt model is clearly favored. This model is also supported by the analysis of the Cu shell at around 3.2\AA (arrows in Fig. 4). Both the amplitude ratio for this shell as well as the calculated distances clearly favor the tilt model. Again, for N^* values of the two expected shells were taken as additive as no beating is observed for this frequency within the experimental k range (see text).

Adsorption state	Fourier peak		Observed	Flat-lying model			Tilt model
				hollow	bridge	atop	
Chemisorbed	1st	N_r	1.1(2)	2.0	1.5	9.7	1.0
	2nd	N_c	0.6(2)	0.8	0.8	0.5	0.7
		R (\AA)	3.2(1)	2.8	2.6	2.6	3.2, 3.3
Physisorbed	1st	N_r	0.9(2)	1.9	2.0	17.	1.1
	2nd	N_c	0.7(2)	0.9	0.9	1.9	0.7
		R (\AA)	3.1(2)	2.7	2.8	2.8	3.1, 3.5

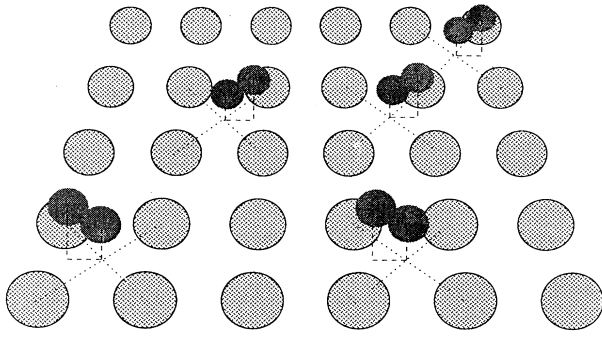


FIG. 6. A schematic representation is shown for the adsorption geometry of the O_2 molecules. The O-O axis is found to make a tilt of $\sim 30^\circ$ from the analysis of the SEXAFS. The NEXAFS data indicate a tilt of $\sim 23^\circ$ for the physisorbed state. One O atom is found to adsorb above a fourfold hollow site the other one almost above a bridge site. This tilted configuration for the O_2 molecules is compatible with a bonding of ionic character to the Cu surface (see text).

still located above the fourfold hollow site. Due to the combined effect of the longer NN distance and shorter O-O bond, the O-O tilt angle remains approximately constant. This value is in good agreement to the value obtained from the NEXAFS data for the physisorbed state ($\sim 23^\circ$). As it can be seen from the values of Table III, the tilt model yields good agreement for the N^* values with the experimental results. This model yields also for the second Fourier peak a distance much closer to experiment. Within the experimental accuracy, no evidence for the existence of two different shells could be observed for this Fourier peak (Table III). This fact can be explained by the strong disorder contributions for the higher shells (noncorrelated motion) combined with the lower signal-to-noise ratio of this feature especially for the physisorbed state. Strong disorder contributions at high- k values damp the expected increase in amplitude due to interference effects.

Having characterized the local geometry for the O_2 molecules, it is of interest to notice that for the atomic precursor state the O atom is still located in the fourfold hollow site.¹¹ The following geometrical picture can then be drawn tentatively concerning the molecular dissociation process: after being trapped in a tilted configuration (physisorption), the O_2 molecule is found mainly "one end" bonded in a strong chemisorbed state, the fourfold hollow O atom being responsible for the strong O-Cu bond. The dissociation process appears to be related then to the loss of the bridge-site O atom, the fourfold hollow-site one remaining anchored in the Cu(100) surface. The previous picture is supported by the analysis of the higher-order PDF moments, discussed in the following section.

D. Determination of the O-Cu pair potentials for the molecular states

In the following, the parameters C_2 and C_3 , the higher moments of the PDF, are taken into account in the

analysis. These higher PDF moments are related to the disorder of the bond under consideration¹⁷⁻²² which can be static or dynamic in nature. As the bond strength increases, the dynamic part of the disorder at a fixed temperature decreases. As shown in Table II, for the chemisorbed state, the fourfold hollow-site O atom has a rather strong bonding with four Cu atoms (bond 1), whose C_2 and C_3 are not very different from that of the precursor state, while the bridge-site O atom is only weakly bonded with the two Cu atoms (bond 2). For the physisorbed state, both bond lengths are apparently identical within the error and very weak.

In order to discuss the bonding nature more quantitatively, we estimate the interatomic potentials for these bonds by using the parameters R , C_2 , and C_3 .^{11,17-19,24} For that purpose the relations between the parameters obtained by EXAFS and the potential parameters need to be given first. For a quasiharmonic one-dimensional quantum oscillator, describing the dynamic part of the disorder and whose potential function $V(r)$ is given by

$$V(r) = \frac{1}{2}\alpha(r-r_0)^2 - \beta(r-r_0)^3, \quad (7)$$

it can be shown that the quantities $R(T)$, $C_2^{\text{dyn}}(T)$, and $C_3^{\text{dyn}}(T)$ (the superscript dyn denotes the dynamic part of the disorder), can be expressed as²⁴

$$R(T) = r_0 + \frac{3\beta}{2\alpha} \left[\frac{\hbar^2}{\mu\alpha} \right]^{1/2} \coth \left[\frac{\Theta_E}{2T} \right], \quad (8)$$

$$C_2^{\text{dyn}}(T) = \frac{1}{2} \left[\frac{\hbar^2}{\mu\alpha} \right]^{1/2} \coth \left[\frac{\Theta_E}{2T} \right], \quad (9)$$

and

$$C_3^{\text{dyn}}(T) = \frac{\beta}{\alpha^2} \left[\frac{\hbar^2}{\mu} \right] \left[\frac{3}{2} \coth^2 \left[\frac{\Theta_E}{2T} \right] - 1 \right], \quad (10)$$

where Θ_E is the Einstein temperature given by $\Theta_E = (1/k_B)[\hbar^2\alpha/\mu]^{1/2}$, μ the reduced mass, k_B the Boltzmann constant, and \hbar the Planck constant divided by 2π . Using the experimentally determined $R(T)$, $C_2^{\text{dyn}}(T)$, and $C_3^{\text{dyn}}(T)$, the potential parameters r_0 , α , and β are evaluated. Furthermore, in order to obtain the potential curves far from the equilibrium, an analytical potential function has to be assumed. Here we employ the Madelung form best suited to describe an ionic bond. The pair potential is given then as

$$V(r) = A \exp \left[-\frac{r-r_0}{B} \right] - \frac{q_a q_s}{r}, \quad (11)$$

where $q_a q_s = Ar_0^2/B$ is the product of the adsorbate and substrate atom charge. The depth of the potential D is given by $D = A(r_0/B - 1)$. Expanding $V(r)$ around r_0 we can obtain the equations

$$\alpha = \frac{A}{B} \left[\frac{1}{B} - \frac{2}{r_0} \right], \quad \beta = \frac{A}{6B} \left[\frac{1}{B^2} - \frac{6}{r_0^2} \right]. \quad (12)$$

These equations allow the determination of the Madelung potential from the EXAFS structural parameters. A

similar approach has been used earlier with success in bulk EXAFS yielding for ionic compounds parameters in a meaningful range.²¹ Recently the use of a Madelung pair potential was also found to yield results for low- Z adsorbates in agreement to theory.^{11,25}

In order to apply the previous formalism and determine $V(r)$, the static part of the disorder needs to be evaluated. This part is known for the atomic precursor state following temperature-dependent SEXAFS studies.¹¹ The results are $C_2^{\text{stat}} = 1.0 \times 10^{-3} \text{ \AA}^2$ and $C_3^{\text{stat}} = 4.0 \times 10^{-4} \text{ \AA}^3$, showing that at the temperature of 50 K the anharmonic contributions for this state are very weak. The Einstein temperature which is obtained for this state by means of Eqs. (5)–(7) is $\Theta_E = 3.6(2) \times 10^2 \text{ K}$.¹¹ For the molecular states studied here, however, a temperature-dependent SEXAFS study is not easily achievable due to the small temperature range, in which they are stable without undergoing a transition to another adsorption state (Fig. 1). Also an inspection of the data of Table I indicates (i) a smooth linear variation of the distance R as a function of the preparation temperature, (ii) a smooth linear increase of the values of ΔC_2 and ΔC_3 as a function of R . Both previous findings do not hold in the case of a variation of the static part of the disorder, as shown for example in the case of the $(\sqrt{2} \times 2\sqrt{2})R45^\circ$ reconstruction.^{11,25} Following the previous observations, for the present analysis we make the assumption that the increase in disorder (ΔC_2 , ΔC_3 in Table I) is only dynamic in nature. This assumption is further supported by the fact that the local geometry for the fourfold hollow-site O-Cu bond for the chemisorbed state is similar to the one of the atomic precursor state. For example, the same value for C_3 is found for these two states, and only a small increase in C_2 is consistent with a slightly stronger O-Cu bond. By using the data of Table II in combination with Eqs. (8)–(10), the Einstein temperatures and pair potentials can be determined for the different O-Cu bonds of the molecular states. We note in particular that for the Einstein temperatures that are obtained (Table IV) using the ΔC_2 values, Eqs. (8)–(10) simplify considerably due to the low temperature used [$\coth(\Theta_E/2T) \approx 1$]. We obtain, for example, for $R(T)$

$$R(T) = r_0 + \frac{3C_3}{2C_2}, \quad (13)$$

to a good approximation. The values of r_0 can then be obtained in a straightforward manner from the data of Table II.

E. Discussion of the adsorption geometry and the dissociation process in terms of pair potentials

Table IV summarizes the determined parameters of the cubic and Madelung O-Cu pair potentials, and Fig. 7 shows the potential curves for the physisorbed and chemisorbed (bonds 1 and 2) and atomic precursor states. As expected, the potential depth for bond 1 in the chemisorbed state is much closer to the one of the precursor state than bond 2, in agreement with the finding that the one oxygen atom is anchored tightly at the hollow site. The potential depth of bond 2 is, on the other hand, almost as shallow as the one of the physisorbed state, indicating almost no chemical bond between the bridge-site oxygen and the Cu atoms. Furthermore, we can roughly estimate the amount of charge transfer from the Madelung parameter $q_a q_s$, where q_s and q_a is the charge of the first-NN Cu and oxygen atom, respectively, and q_s can be assumed to be $q_s \approx q_a/2$ since the saturated coverage for both chemisorbed and precursor states are around 0.5 ML by making the simplifying assumption that only the surface Cu layer is charged. The calculated value for q_a is 0.66e for bond 1 for the chemisorbed state, a value smaller than the one of the precursor state ($q_a \approx 0.87e$).¹¹ On the contrary, for bond 2 in the chemisorbed state, q_a is only 0.16e and for the physisorbed state ($q_s \approx q_a/0.7$), q_a is 0.11e. These results indicate that in the chemisorbed state the fourfold hollow-site oxygen is strongly negatively charged exhibiting a strong ionic bonding with the Cu atoms, while the bridge-site oxygen is nearly neutral and its bonding is as weak as the one of the physisorbed state.

A further inspection of the data of Fig. 7 and Table IV shows that the O-Cu interatomic distance in the physisorbed state is not very different from that in the chemisorbed state, while the potential depth of bond 1 in the chemisorbed state (fourfold hollow site) is significantly different. There is, however, another structural parameter that allows to distinguish these two molecular states: the O-O intramolecular distance, as was previously discussed (Sec. III) is strongly varying between the two

TABLE IV. The Einstein temperatures and Madelung potential parameters for the first NN O-Cu pairs of the precursor (Ref. 11), chemisorbed and physisorbed states are given. The potential parameters were determined using the data of Table II and Eqs. (7)–(13). The parameters r_0 give the potential minimum, B determines the strength of the repulsive part, and D is the potential depth. Instead of listing the parameters $q_a q_s$ we give the values of q_a (the adsorbate atom ionic charge) in units of the electron charge. These were obtained by assuming that this ionic charge was delivered by the first-layer Cu atoms only. The coverage of the different adsorption states (Secs. II and III) was taken into account.

Adsorption state		Θ_e (10^2 K)	r_0 (\AA)	B (\AA)	D (eV)	q_a/e
Precursor		3.6(2)	1.85(3)	0.34(3)	2.4(3)	0.87(10)
Chemisorbed	Bond 1	3.0(3)	1.97(3)	0.28(3)	1.4(5)	0.66(10)
	Bond 2	1.5(2)	1.96(4)	0.08(1)	0.09(3)	0.16(5)
Physisorbed		1.4(2)	1.96(4)	0.06(1)	0.06(2)	0.11(5)

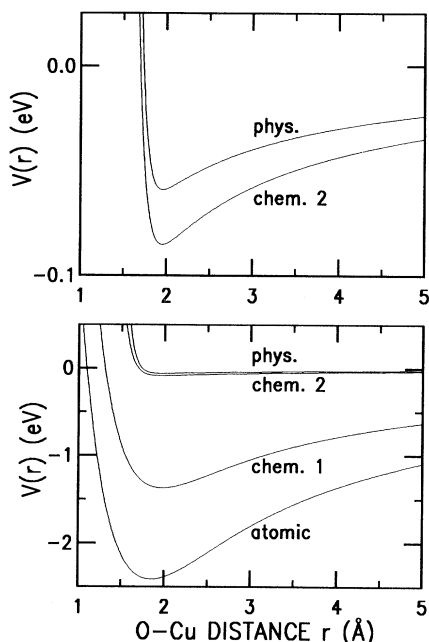


FIG. 7. The Madelung pair potentials are shown for the different O-Cu bonds. It is observed that from the physisorbed to the chemisorbed state no big O-Cu distance variation is found, in contrast to the other potential parameters which are found to vary strongly. This observation is consistent with theoretical calculations (see text). Furthermore this insensitivity of the O-Cu NN bond length with respect to the dissociation process appears to hold beyond dissociation as a comparison of the results of the chemisorbed state with respect to the atomic states indicates.

states. In the physisorbed state, the electronic structure of the adsorbed oxygen molecules is nearly gas-phase-like, with an O-O distance of 1.21 Å. On the contrary, for the chemisorbed state, the O-O bond is weaker with an elongated distance of 1.52 Å, compatible with a much stronger interaction between the O₂ molecule and the Cu substrate. It is of interest to compare the previous findings with theoretical calculations. As no calculations on the dissociation of O₂ on a Cu surface are available, we turn to the well-studied O₂/Ag(110) system.⁹ For this system also a strong chemisorption is found and an O-O bond of ~1.5 Å. It is also found that the O-Ag distance remains almost unchanged as the strength of chemisorption increases.⁹ Furthermore the charge transfer to the O₂ molecule was found to be ~0.9 electron. Our results indicate also a similar O-O distance and a total charge on the O₂ molecule of 0.8(1) electron, close to the calculated value. The good agreement with the theoretical results gives confidence in the self-consistency of the analysis and the validity of the simplifying assumption of a predominantly ionic interaction. Further support for an

ionic interaction is given by the tilted configuration of the O₂ molecules. Recent calculations on the adsorption of NO on Cu(111), tie the tilted configuration of this species to an ionic bond with the surface (NO⁻).²⁶ A tilted configuration appears to be of advantage for the little orientational ionic interaction which permits the center of the negative charge to be closer to the surface.²⁶ This would also be the case for the O₂ molecule, which is found to adsorb in a tilted configuration not only on Cu(100) but on Ag(110) as well.⁴ Our data also indicate that with a further temperature rise in the transition from the chemisorbed to the atomic state, the hollow-site oxygen does not move very much: only a slight inward displacement takes place because of the slight shortening of the O-Cu bond distance, while the bridge-site oxygen might move away in order to occupy another fourfold hollow site.

V. CONCLUSIONS

By combining the results of NEXAFS, XPS, and TDS the sequential molecular adsorption of oxygen molecules on Cu(100) as a function of temperature has been characterized. It is of importance to stress the prototypical character of the present study, as it is the first time to our knowledge that the SEXAFS of physisorbed molecules could be measured and analyzed. The data analysis is based on a relative comparison of the NN O-Cu bond contribution to the SEXAFS for several adsorption states. The NEXAFS data indicate that the O₂ molecules adsorb in a tilted configuration in agreement to the local geometry obtained by means of the SEXAFS. Furthermore the SEXAFS data indicate that the O₂ molecules adsorb with one atom occupying a fourfold hollow site, the other being situated close to a bridge site. The two close-lying Cu shells corresponding to these two sites were resolved for the molecules in the chemisorbed state. It is found that the molecular dissociation process occurs with little change in the O-Cu distance in opposition to strong changes in all other O-Cu pair-potential parameters and O-O bond length. The higher moments of the SEXAFS data could be analyzed by making reasonable assumptions on the static part of the disorder and assuming an ionic interaction to the substrate, consistent with the molecular adsorption in a tilted configuration.

ACKNOWLEDGMENTS

We would like to thank J. Stöhr for helpful and stimulating discussions and H. Rabus for help during the measurements. This project was supported by the German BMFT (Grant No. 05 5KEAAB) and the European LSI program (Grant No. EG 033-1500290). One of the present authors (T.Y.) is grateful for the financial support of the Alexander von Humboldt Foundation.

- *On leave from the Department of Materials Science, Hiroshima University, Kagamiyama, Higashi-Hiroshima, Hiroshima 724, Japan.
- ¹A. C. Luntz, J. Grimblot, and D. E. Fowler, *Phys. Rev. B* **39**, 12 903 (1989).
- ²D. A. Outka, J. Stöhr, W. Jark, P. Stevens, J. Solomon, and R. J. Madix, *Phys. Rev. B* **35**, 4119 (1987).
- ³W. Wurth, J. Stöhr, P. Feulner, X. Pan, K. R. Bauchspiess, Y. Baba, E. Hudel, G. Rocker, and D. Menzel, *Phys. Rev. Lett.* **65**, 2426 (1990).
- ⁴R. J. Guest, B. Hernnäs, P. Bennich, O. Björneholm, A. Nilsson, R. E. Palmer, and N. Martensson, *Surf. Sci.* **278**, 239 (1992).
- ⁵C. T. Campbell, *Surf. Sci.* **157**, 43 (1985).
- ⁶B. A. Sexton and R. J. Madix, *Chem. Phys. Lett.* **76**, 294 (1980).
- ⁷C. Backx, C. P. M. de Groot, and P. Biloen, *Surf. Sci.* **104**, 300 (1981).
- ⁸T. H. Upton, P. Stevens, and R. J. Madix, *J. Chem. Phys.* **88**, 3988 (1988).
- ⁹P. J. Van der Hoek and E. J. Baerends, *Surf. Sci.* **221**, L791 (1989).
- ¹⁰U. Döbler, K. Baberschke, J. Stöhr, and D. A. Outka, *Phys. Rev. B* **31**, 2532 (1985).
- ¹¹T. Lederer, D. Arvanitis, G. Comelli, L. Tröger, and K. Baberschke, preceding paper, *Phys. Rev. B* **48**, 15 390 (1993).
- ¹²J. Stöhr and D. A. Outka, *Phys. Rev. B* **36**, 7891 (1987).
- ¹³A. P. Hitchcock and C. E. Brion, *J. Electron Spectrosc.* **18**, 1 (1980).
- ¹⁴N. Kosugi, E. Shigemasa, and A. Yagishita, *Chem. Phys. Lett.* **190**, 481 (1992).
- ¹⁵F. Sette, J. Stöhr, and A. P. Hitchcock, *J. Chem. Phys.* **81**, 4906 (1984).
- ¹⁶R. J. Guest, A. Nilsson, O. Björneholm, B. Hernnäs, A. Sandell, R. E. Palmer, and N. Martensson, *Surf. Sci.* **269/270**, 432 (1992).
- ¹⁷See, for example, *X-Ray Absorption: Principles, Application, Techniques of EXAFS, SEXAFS and XANES*, edited by D. C. Koningsberger and R. Prins (Wiley, New York, 1988).
- ¹⁸G. Bunker, *Nucl. Instrum. Methods* **207**, 437 (1983).
- ¹⁹L. Wenzel, D. Arvanitis, H. Rabus, T. Lederer, and K. Baberschke, *Phys. Rev. Lett.* **64**, 1765 (1990).
- ²⁰J. M. Tranquada and R. Ingalls, *Phys. Rev. B* **28**, 3520 (1981).
- ²¹T. Yokoyama, T. Satsukawa, and T. Ohta, *Jpn. J. Appl. Phys.* **28**, 1905 (1989).
- ²²E. A. Stern, P. Livins, and Z. Zhang, *Phys. Rev. B* **43**, 8850 (1991).
- ²³L. Tröger, D. Arvanitis, J. J. Rehr, T. Lederer, T. Yokoyama, K. Baberschke, and E. Zschech, *Jpn. J. Appl. Phys.* **32**, 137 (1993).
- ²⁴H. Rabus, Ph.D. thesis, Freie Universität, Berlin, 1991.
- ²⁵D. Arvanitis, T. Lederer, G. Comelli, M. Tischer, T. Yokoyama, L. Tröger, and K. Baberschke, *Jpn. J. Appl. Phys.* **32**, 337 (1993).
- ²⁶M. Fernandez-Garcia, J. C. Conesa, and F. Illas, *Surf. Sci.* **280**, 441 (1993).